# Supporting Information

# Optimizing the Synthetic Conditions of "Green" Colloidal $AgBiS_2$ Nanocrystals Using Low-Cost Sulfur Source

**Qiao Li [1], Xiaosong Zheng [1], Xiaoyu Shen [1], Shuai Ding [1], Hongjian Feng [1,*], Guohua Wu [2,*], Yaohong Zhang [1,3*]**

[1] School of Physics, Northwest University, Xi'an 710127, China

[2] Qingdao Innovation and Development Base of Harbin Engineering University, Harbin Engineering University, Heilongjiang 150001, China

[3] Shaanxi Key Laboratory for Carbon Neutral Technology, Xi'an 710127, China

*Corresponding authors:

Yaohong Zhang: yhzhang@nwu.edu.cn

Hong-Jian Feng: hjfeng@nwu.edu.cn

Guohua Wu: ghwu@hrbeu.edu.cn

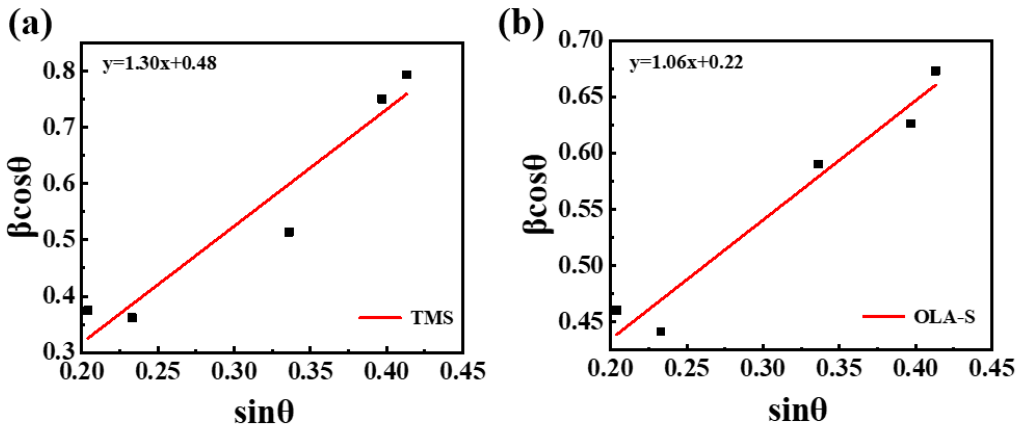


**Figure S1.** The William-Hall plots for (a) TMS-based and (b) OLA-S-based colloidal $AgBiS_2$ NCs.

The relationship between full width at half maximum of XRD peak ($\beta$) and lattice strain ($\varepsilon$) follows the Williamson-Hall equation: [1,2]

$$\beta \cos\theta = 4\varepsilon \sin\theta + \frac{K\lambda}{D_{size}} \qquad \text{eq. (1)}$$

where $\theta$ is the Bragg angle in radian, $K$ is the sharp factor (K=0.94), $\lambda$ is the wavelength of X-ray ($CuK_\beta$) in nanometers ($\lambda$=0.14 nm), and $D_{size}$ is the average NC size in nanometers, respectively. The lattice strain, $\varepsilon$, can be evaluated from the slope of the linear fitting of the data when $\beta\cos\theta$ is plotted on the y axis and $\sin\theta$ is plotted on the x axis. The fitting results are shown in Table S1.

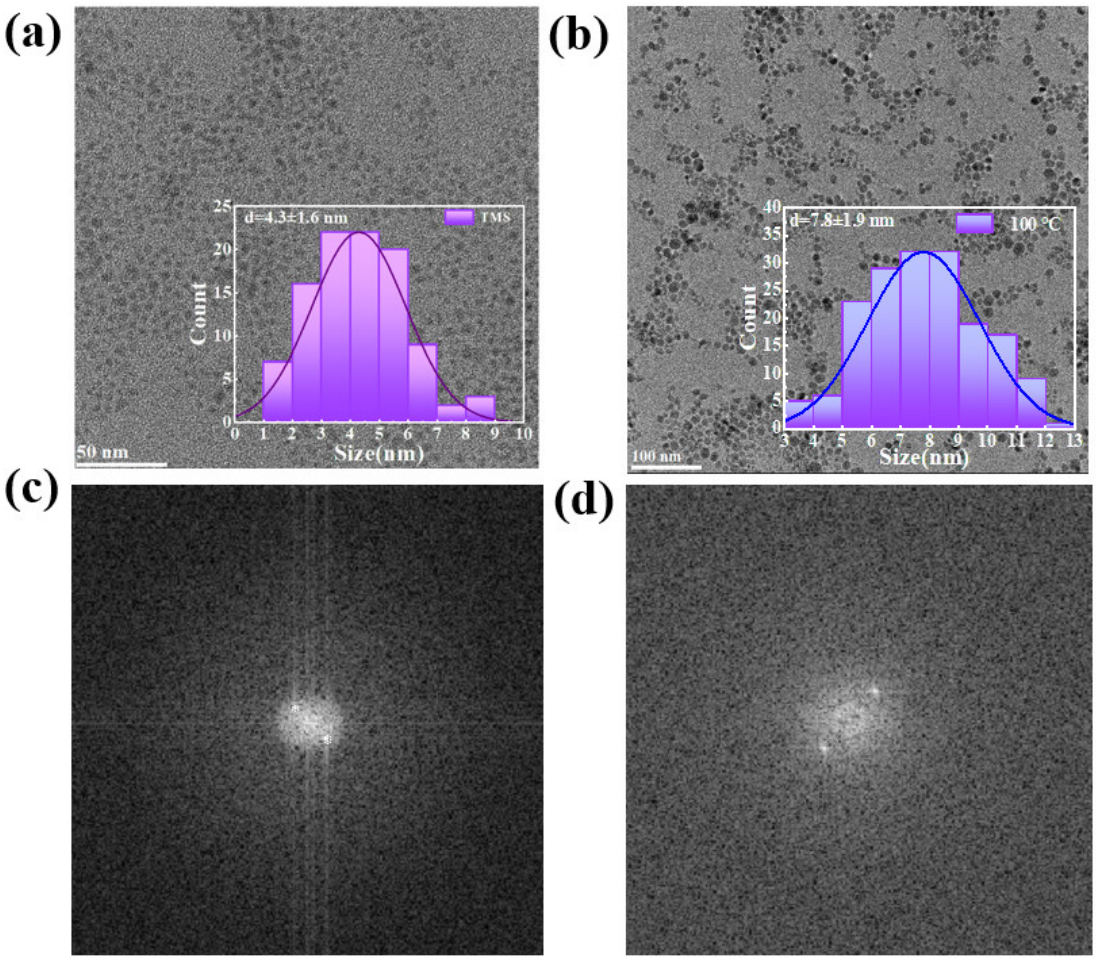


**Figure S2.** TEM images of (a) TMS-based and (b) OLA-S-based colloidal $AgBiS_2$ NCs. Insets are the statistical histograms of the NCs size distribution. SAED images of (c) TMS-based and (d) OLA-S-based colloidal $AgBiS_2$ NCs.

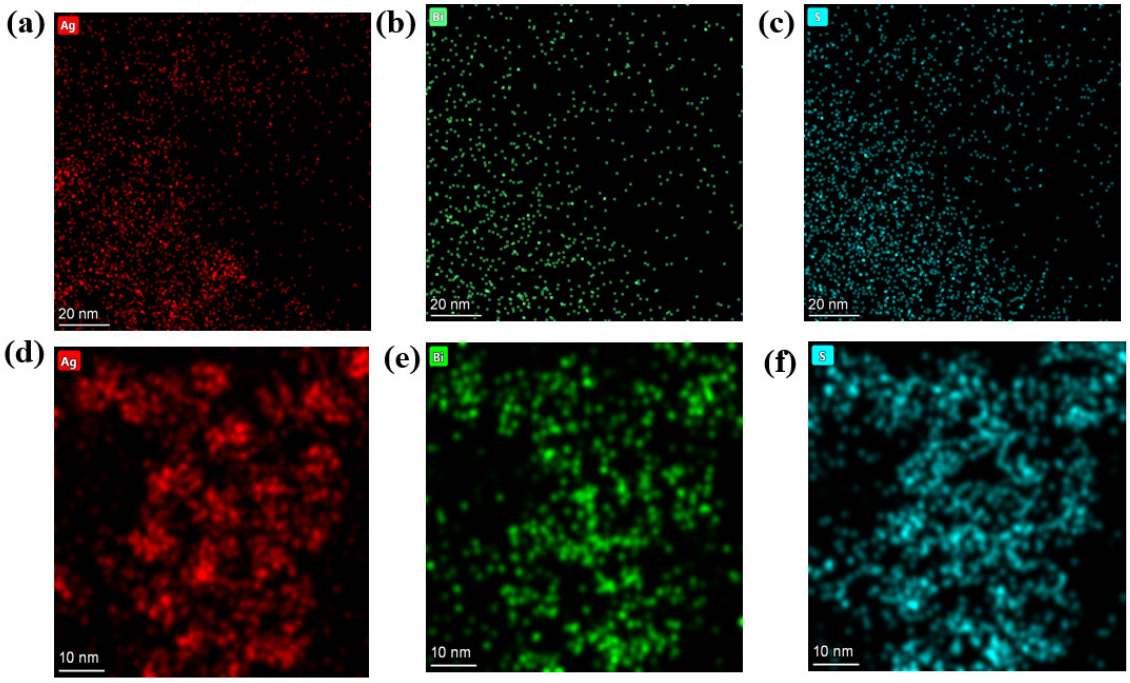


**Figure S3.** EDS-Mapping images of (a) Ag, (b) Bi and (c) S of TMS-based. EDS-Mapping images of (d) Ag, (e) Bi and (f) S of OLA-S-based colloidal $AgBiS_2$ NCs.

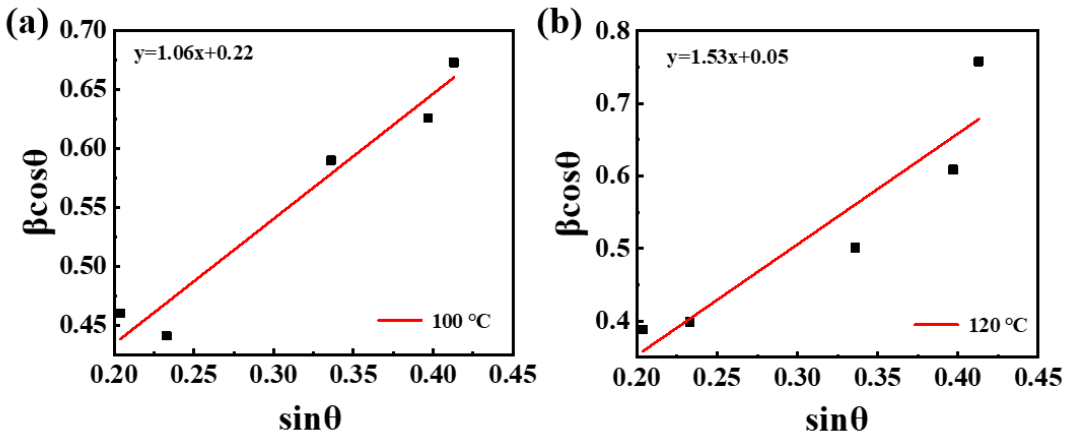


**Figure S4.** The William-Hall plots for OLA-S-based colloidal $AgBiS_2$ NCs prepare at (a) 100°C and (b) 120°C.

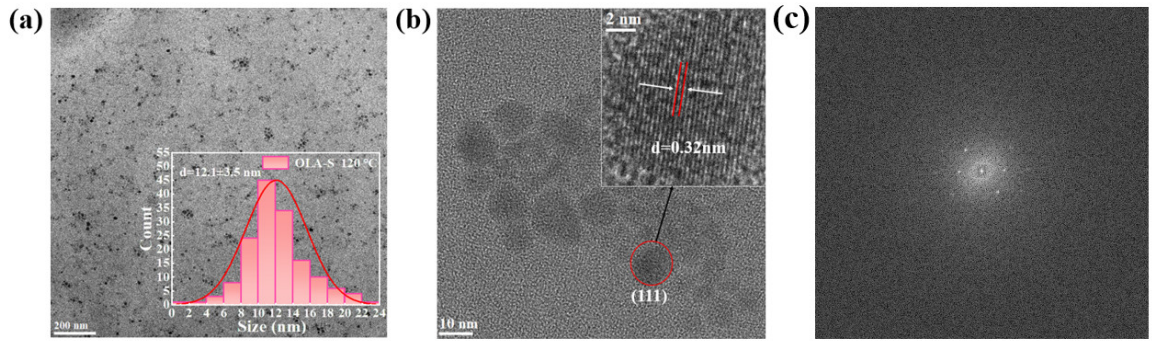


**Figure S5.** TEM images of (a) OLA-S-based colloidal $AgBiS_2$ NCs prepare at 120°C. Insets are the statistical histograms of the NCs size distribution. (b) HR-TEM images of OLA-S-based colloidal $AgBiS_2$ NCs prepare at 120°C. (c) SAED image of OLA-S-based colloidal $AgBiS_2$ NCs prepare at 120°C.

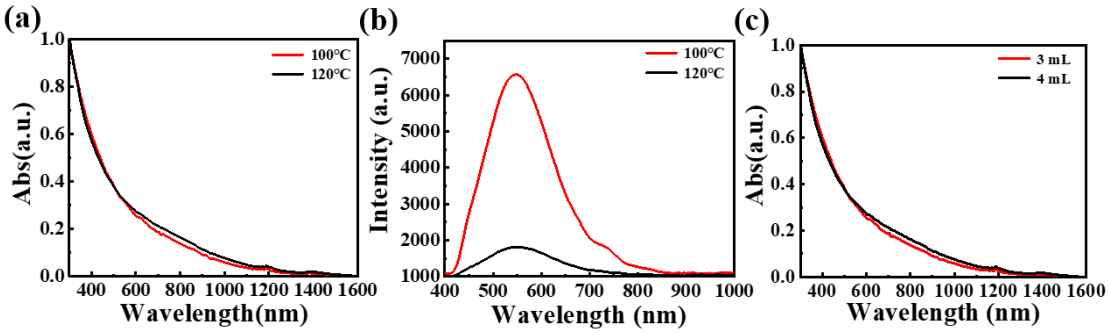


**Figure S6.** (a) UV−vis−NIR absorption spectra of the colloidal $AgBiS_2$ NCs in hexane. (b) PL spectrum and fitting curves of OLA-S-based colloidal $AgBiS_2$ NCs prepare at 100°C and 120°C. (c) UV−vis−NIR absorption spectra of the 3 mL and 4 mL colloidal $AgBiS_2$ NCs in hexane.

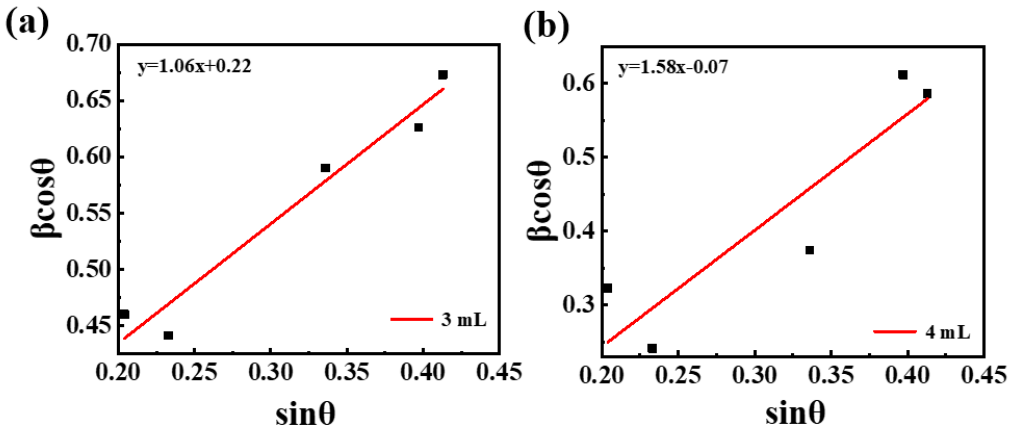


**Figure S7.** The William-Hall plots for (a) 3 mL and (b) 4 mL OLA-S-based colloidal $AgBiS_2$ NCs.

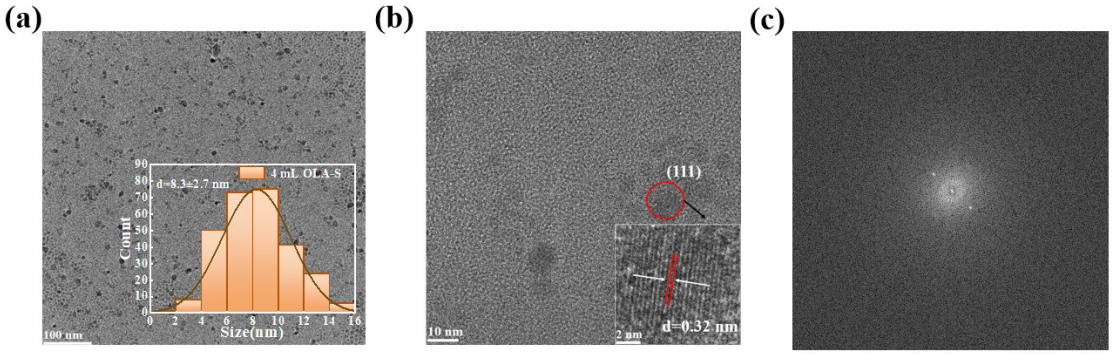


**Figure S8.** TEM images of (a) 4 mL OLA-S-based colloidal $AgBiS_2$ NCs. Insets are the statistical histograms of the NCs size distribution. (b) HR-TEM images of 4 mL OLA-S-based colloidal $AgBiS_2$ NCs. (c) SAED image of 4 mL OLA-S-based colloidal $AgBiS_2$ NCs.

**Table S1.** Half-peak widths and lattice strains of OLA-S-based and TMS-based colloidal $AgBiS_2$ NCs.

| Sulfur source | Crystal plane | Half-peak wide(nm) | Lattice strain |
|---|---|---|---|
| OLA-S | (111) | 3.51 | 0.27 |
| | (200) | 2.95 | |
| | (220) | 2.73 | |
| | (311) | 3.45 | |
| | (222) | 2.53 | |
| TMS | (111) | 2.81 | 0.33 |
| | (200) | 2.50 | |
| | (220) | 4.06 | |
| | (311) | 4.34 | |
| | (222) | 2.66 | |

**Table S2.** Half-peak widths and lattice strains of OLA-S-based colloidal $AgBiS_2$ NCs prepare at 100°C and 120°C.

| Temperature (℃) | Crystal plane | Half-peak wide(nm) | Lattice strain |
|---|---|---|---|
| 100℃ | (111) | 3.51 | 0.27 |
| | (200) | 2.95 | |
| | (220) | 2.73 | |
| | (311) | 3.44 | |
| | (222) | 2.53 | |
| 120℃ | (111) | 2.96 | 0.38 |
| | (200) | 2.66 | |
| | (220) | 2.32 | |
| | (311) | 2.38 | |
| | (222) | 2.29 | |

**Table S3.** Half-peak widths and lattice strains of 3 mL and 4 mL OLA-S-based colloidal $AgBiS_2$ NCs.

| Temperature (℃) | Crystal plane | Half-peak wide(nm) | Lattice strain |
|---|---|---|---|
| 3 mL | (111) | 3.51 | 0.27 |
| | (200) | 2.95 | |
| | (220) | 2.73 | |
| | (311) | 3.44 | |
| | (222) | 2.53 | |
| 4 mL | (111) | 2.46 | 0.40 |
| | (200) | 1.60 | |
| | (220) | 1.73 | |
| | (311) | 2.39 | |
| | (222) | 2.20 | |

**Table S4.** Raw material usage, price and yield of $AgBiS_2$ NCs based on TMS and OLA-S.

| Sulfur Source | Raw Material | Synthetic Usage | Price(yuan) | Total(yuan) | Yield(%) |
|---|---|---|---|---|---|
| TMS | $Bi(OAc)_3$ | 386 mg | 24.5 | 80.4 | (265 mg) 86.9 |
| | AgOAc | 134 mg | 3.0 | | |
| | OA | 5.4 mL | 4.3 | | |
| | ODE | 15 mL | 2.6 | | |
| | TMS | 215 μL | 46.0 | | |
| OLA-S | $Bi(OAc)_3$ | 386 mg | 24.5 | 34.8 | (276 mg) 90.5 |
| | AgOAc | 134 mg | 3.0 | | |
| | OA | 5.4 mL | 4.3 | | |
| | ODE | 10 mL | 1.8 | | |
| | OLA | 3 mL | 1.2 | | |
| | S | 96 mg | 0.003 | | |

## Reference


1. Williamson, G. K.; Hall, W. H. X-ray line broadening from filed aluminium and wolfram L'elargissement des raies de rayons x obtenues des limailles d'aluminium et de tungsten Die verbreiterung der roentgeninterferenzlinien von aluminium- und wolframspaenen, *Acta Metallurgica* **1953**, *1*, 22-31.

2. Nishimura, K.; Hirotani, D.; Kamarudin, M. A.; Shen, Q.; Toyoda, T.; Iikubo, S.; Minemoto, T.; Yoshino, K.; Hayase, S. Relationship between lattice strain and efficiency for Sn-perovskite solar cells, *ACS Appl. Mater. Interfaces* **2019**, *11*, 31105-31110.